University Library



A gateway to Melbourne's research publications

Minerva Access is the Institutional Repository of The University of Melbourne

Author/s:
Seyler, H;Purushothaman, B;Jones, DJ;Holmes, AB;Wong, WWH

Title:
Hexa-peri-hexabenzocoronene in organic electronics

Date:
2012-01-01

Citation:
Seyler, H., Purushothaman, B., Jones, D. J., Holmes, A. B. & Wong, W. W. H. (2012). Hexa-peri-hexabenzocoronene in organic electronics. PURE AND APPLIED CHEMISTRY, 84 (4), pp.1047-1067. https://doi.org/10.1351/PAC-CON-11-09-24.

Persistent Link:
https://hdl.handle.net/11343/32675

Pure Appl. Chem., Vol. 84, No. 4, pp. 1047–1067, 2012.
http://dx.doi.org/10.1351/PAC-CON-11-09-24
© 2012 IUPAC, Publication date (Web): 13 March 2012

Hexa-*peri*-hexabenzocoronene in organic electronics*

Helga Seyler, Balaji Purushothaman, David J. Jones, Andrew B. Holmes, and Wallace W. H. Wong‡

School of Chemistry, Bio21 Institute, University of Melbourne, 30 Flemington Road, Parkville, Victoria 3010, Australia

Abstract: Polycyclic aromatic hydrocarbons (PAHs) are in a class of functional organic compounds with increasing importance in organic electronics. Their tunable photophysical properties and typically strong intermolecular associations make them ideal materials in applications where control of charge mobility is essential. Hexa-*peri*-hexabenzocoronene (HBC) is a disc-shaped PAH that self-associates into columnar stacks through strong π–π interactions. By decorating the periphery of the HBC molecule with various substituents, a range of properties and functions can be obtained including solution processability, liquid crystallinity, and semiconductivity. In this review article, the synthesis, properties, and functions of HBC derivatives are presented with focus on work published in the last five years.

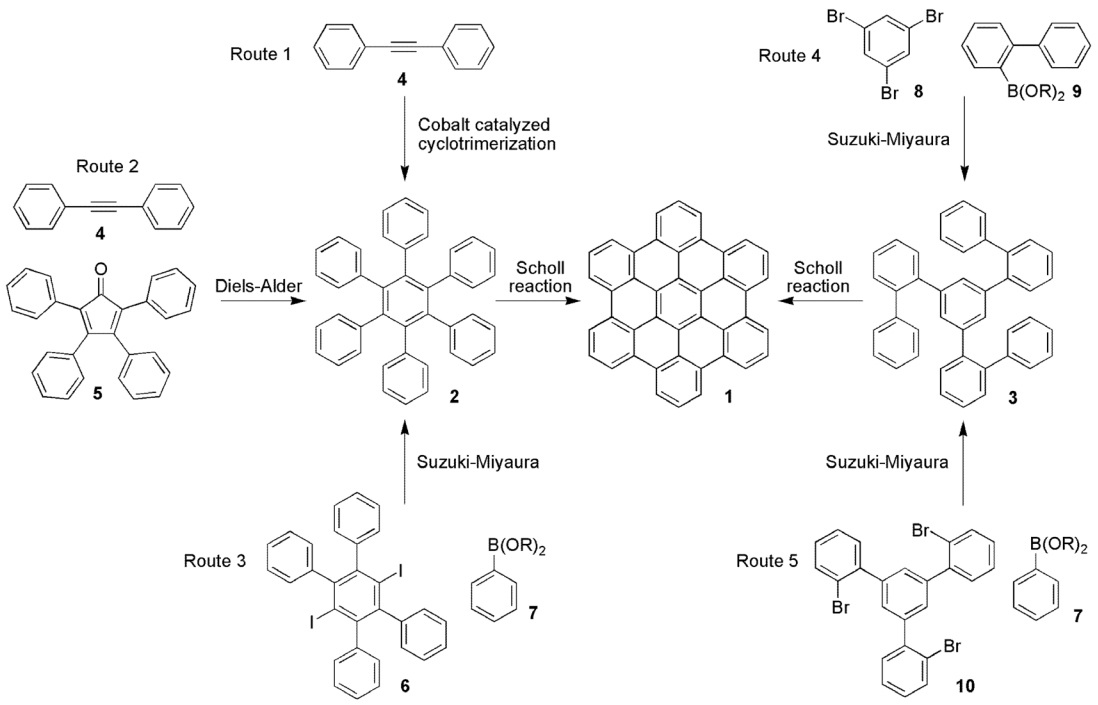
Keywords: hexabenzocoronene; materials chemistry; molecular electronics; organic electronics; organic semiconductors; photovoltaics; polycyclic aromatics; self-organization.

INTRODUCTION

Polycyclic aromatic hydrocarbons (PAHs) are defined as fused ring materials consisting of sp^2 carbon centers and can be considered as segments of graphite. The dominant intermolecular force is often face-to-face π–π interactions with some examples of face-to-edge (or herringbone) assembly. Although PAHs can often be found naturally in combustion residues, analytically pure and discrete PAHs can only be obtained through synthesis. PAHs, with a variety of molecular shapes and sizes, have now been synthesized. This includes linear structures, such as pentacene, to two-dimensional shapes, such as perylene [1,2]. Many PAHs have been used as functional materials. For example, pentacene is one of the most well-known PAHs and has been extensively used in organic field effect transistors (OFETs) [3,4]. Strong intermolecular forces and a high degree of molecular order in pentacenes films result in high charge carrier mobility, a key determinant in OFET device performance. There have also been a number of studies of large PAH structures [1,5]. Large PAH structures are potential electrode materials with properties closely related to infinitely large PAH sheets, or graphenes.

Hexa-*peri*-hexabenzocoronene (HBC) is a discotic PAH consisting of 42 carbon atoms (Scheme 1, **1**). HBC molecules are highly stable with strong intermolecular forces driving self-assembly. Its disc shape means that HBCs most commonly form columnar structures through π–π stacking. As a result of the strong intermolecular forces, the HBC molecule **1** is an insoluble material which can be processed by vacuum deposition. Functionalized HBC derivatives can be solution processed and can

Pure Appl. Chem.* **84, 861–1112 (2012). A collection of invited papers based on presentations at the 14th International Symposium on Novel Aromatic Compounds (ISNA-14), Eugene, OR, USA, 24–29 July 2011.
‡Corresponding author



Scheme 1 Various synthetic routes toward the HBC core molecule. Functional groups around the HBC core are omitted for clarity.

exhibit a range of properties including liquid crystallinity. Synthetic versatility also allows for a large variation in functional groups on the HBC molecule. This has led to potential applications as nanostructured materials in biology, energy storage, and organic electronics. In this article, the synthesis of HBC derivatives will be discussed with a focus on literature in the last five years. This will be followed by a review of self-assembly properties of HBCs and the influence of functional groups. Finally, the role of HBCs as a functional material will be discussed with emphasis on organic electronic applications.

SYNTHESIS OF HBC AND ITS DERIVATIVES

The development of HBC synthesis since the first publication by Clar and co-workers [6] has been covered in detail in previous reviews [5]. Synthesis of most HBC derivatives in the last decade has largely been developed by Müllen and co-workers. As early as 1995, a milder synthetic approach to alkyl-substituted HBCs has been reported involving the treatment of functionalized hexaphenylbenzene (HPB) **2** with Cu(II) and Al(III) salts as oxidant and Lewis acid, respectively [7,8]. The enhanced solubility of alkylated HBCs enabled their purification and characterization. The HPB core can be assembled using the functional group tolerant dicobaltcarbonyl-catalyzed cyclotrimerization of 1,2-diphenylethyne **4** (Scheme 1, route 1) [9–11]. It was possible to obtain C3-symmetric HBC from asymmetric tolanes carrying esters and alkyl substitutents using this approach (Scheme 1, route 1) [12]. The cobalt-promoted cyclotrimerization yielded thus two regioisomers of the HPB, which were easily separated prior to cyclodehydrogenation. The HPB and HBC with alkyl and ester side chains tethered in an alternating substitution pattern were isolated in 63 % and over 85 %, respectively. Similarly, the same method was applied to a C3-symmetric trimethoxy HBC with alkyl chains, although methoxy migration and spirocyclic dienone formation lead to poor yields of the desired HBC [13]. Regiocontrol of functional groups

around the HBC core was achieved via [4+2] Diels–Alder cycloaddition route (Scheme 1, route 2) [14,15]. The addition of the acetylene **4** to the cyclopentadienone **5** gave a carbonyl bridge intermediate which undergoes carbon monoxide elimination to give the corresponding HPB. The HPB core can also be assembled via Suzuki–Miyaura cross-coupling of sterically hindered 1,4-diiodo-2,3,5,6-tetraarylbenzenes **6** with functionalized boronic esters **7** yielding D2-symmetric HBCs after planarization (Scheme 1, route 3) [16]. An alternative route to C3-symmetric HBCs involves the Suzuki coupling of 1,3,5-tribromobenzene **8** with biphenyl boronic acid **9** (Scheme 1, route 4) [17]. The obtained 1,3,5-tris(2'-biphenyl)benzene **3** can be submitted to mild cyclodehydrogenation conditions to give parent HBC. This route has been used to access alkoxylated HBCs in nearly quantitative yield [18]. The Suzuki coupling of 1,3,5-tris(bromophenyl)benzene **10** with aryl boronic acid derivatives **7** also led to C3-symmetric HBC compounds (Scheme 1, route 5) [19].

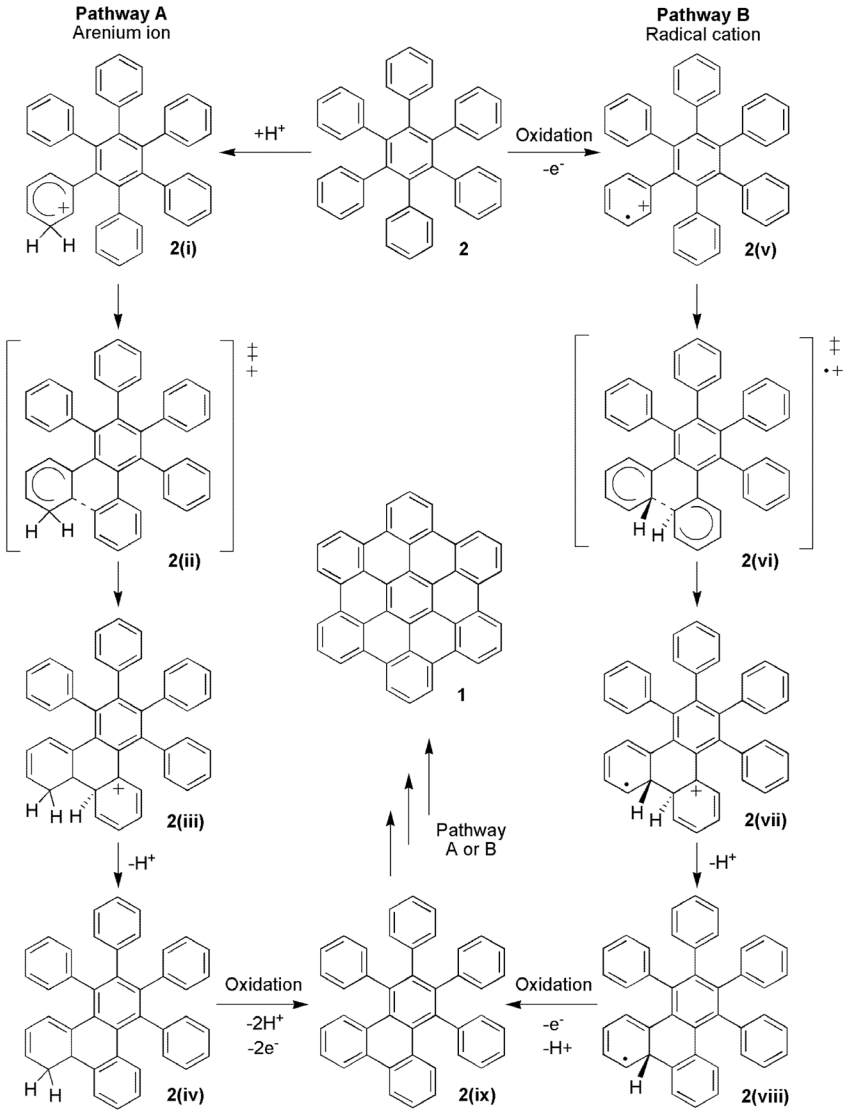
From all synthetic approaches to HBCs that have been developed during the last century, the oxidative aryl-aryl coupling under the influence of Lewis acids, or Scholl reaction, remains the crucial step [20,21]. Early procedures using NaCl/$AlCl_3$ limited the scope of the cyclodehydrogenation reaction owing to its harsh conditions. The development of alternative methods under milder conditions paved the way for functional group diversity in HBCs. Enormous progress in the preparation of functionalized HBCs was made with the development of the Fe(III) chloride/nitromethane promoted cyclodehydrogenation in excellent yields and under mild conditions [14,15]. The use of Fe(III) as Lewis acid and oxidant significantly reduced side reactions such as alkyl chain migration, dealkylation, or chlorination. In addition, strategically functionalized HPB halide precursors can easily be obtained, enabling further chemical modification to yield a large variety of derivatives [5]. Alternative protocols describe the use of $AlCl_3$ in combination with Cu(II) salts (chloride or triflate) [22], dichlorodicyano-*p*-benzoquinone (DDQ) in the presence of an acid [23], $MoCl_5$, and $PhI(O_2CCF_3)_2/BF_3$-Et_2O [24].

The scope of the Scholl-type reaction with HPB precursors ranges from the preparation of insoluble unsubstituted, hexakis-halides (I, F) HBCs [25,26] to soluble derivatives carrying alkyl (chiral, linear, branched), alkylphenyl, iodophenyl, or mono/multiple bromide [5], iodofluorenes [27], methylene iodide [28], and heteroaromatics [29] on the periphery. Tris(biphenyl)benzene substrates were transformed to the corresponding trialkyl [30], hexakis-alkoxy [18], or triiodo [19] HBCs. Limitations for this transformation are encountered when substituents are chemically incompatible with the reaction conditions or when reaction intermediates become stabilized. Moreover, some particular target compounds were only obtainable from specifically designed isomeric precursors. For example, attempts to prepare alkoxy-functionalized HBCs from the corresponding HPB via oxidative cyclization with $FeCl_3$ led to variable results with byproducts from alkoxy migrations [31], quinine [32], or indenofluorene [13,18] formation. However, a hexakis-alkoxy-HBC was accessible from a 1,3,5-tris(biphenyl)benzene derivative **3** [18] or when a phenyl linker is incorporated (Scheme 1, route 4) [33–36]. Ketone and ester functional groups such as alkan-1-ones, alkoxycarbonyl and methylene carboxy alkanoate have been reported incompatible with $FeCl_3$ cyclohehydrogenation conditions [37]. Interestingly, a *tert*-butyl-substituted 1,4-bis-(2'-biphenyl)yl-2,5-diphenylbenzene precursor required repeated $FeCl_3$ treatment to arrive at the fully cyclodehydrogenated product [19], whereas the presence of four, five, or six *tert*-butyl solubilizing chains in HPBs gives HBCs in good to excellent yields with $FeCl_3$ or DDQ [23,38,39].

In general, electron-withdrawing (as nitriles or carbonyls) or donor (as alkoxy or amines) substituents hinder the planarization reaction [28]. However, introduction of spacers or additional peripheral substituents, which counteract the undesired electronic effect, can improve the outcome of the reaction. Thus, trifluoromethyl substitution on HPB precursors does not lead to the decyclohydrogenated product, but fluorine atoms directly attached to the core [26] and fluorinated alkyl chains connected via an aliphatic linker afford good yields [40,41]. Hexakis(4-bromophenyl)benzene failed to give the corresponding fully cyclodehydrogenated product under any oxidative condition [37,42].

In HBC synthesis via the oxidative cyclodehydrogenation (Scholl) reaction, the usual byproducts resulted from chlorination and polymerization side reactions, but those can typically be minimized by

passing a constant stream of inert gas through the solution to remove formed gaseous hydrochloric acid or by adjusting the stoichiometry of the reagents. A stepwise cyclization mechanism has been suggested for HBC formation as semifused HPB derivatives were sometimes isolated as byproducts [8,35]. Two disputed mechanisms for the Scholl reaction have been proposed and investigated: the arenium-ion or radical-cation pathways (Scheme 2) [24,31,43–46]. The former (Scheme 2, pathway A) proceeds by protonation of the aromatic precursor, resulting in a σ complex or arenium cation **2(i)**. Electrophilic attack on an arene under generation of a new C–C bond, deprotonation, and subsequent oxidation affords the condensed product **2(ix)**. In contrast, the radical cation **2(v)** (Scheme 2, pathway B) is generated by one-electron oxidation. Electrophilic C–C bond formation with a second arene gives intermediate **2(vii)**. After one proton elimination and re-aromatization of one six-carbon ring, one-electron oxidation and deprotonation follows on the second ring to afford the fused product **2(ix)**. This radical



Scheme 2 Proposed arenium-cation (pathway A) and radical-cation (pathway B) mechanisms for the conversion of HPB to HBC in the Scholl reaction.

mechanism is supported by Negri [46] under $CuCl_2/AlCl_3$ reaction conditions and by Rathore [42] using DDQ as oxidant. On the other hand, experimental and computation studies under various Kovacic conditions support the arenium-ion pathway [24,45].

With the synthetic tools to form the HBC core, the variety of substituents on the HBC molecule is virtually limitless. Several reviews and papers have summarized the structural diversity of HBC derivatives [5,47–49]. In terms of different regio-functionalizations, 6-, 12- and 18-fold functionalization of HBCs is straightforward and a number of different solubilizing groups have been reported (Fig. 1a, **11** and **12**). HBCs can also be decorated with reactive substituents such as aryl halides to install additional functional groups via coupling reactions [37]. Extension of π-conjugation with acetylenes, phenyl- and diphenylacetylenes carrying nonpolar or polar alkyl chains are encountered in the literature [5,47–49]. By attaching lipophilic, hydrophilic, and fluorous solubilizing groups to the HBC core, it is possible to produce amphiphilic materials (Fig. 1b, **13**). Particular success in the control of supramolecular assembly has been achieved for the Gemini-shaped amphiphilic HBCs (Fig. 1c, **14**) [34,50]. Further structural complexity has been achieved by functionalization of the HBC periphery (directly or indirectly through spacer groups) with chemically reactive, electrochemically responsive, and photoactive substituents [5,47–49]. In the following section, the most recent and functional HBC derivatives will be highlighted.

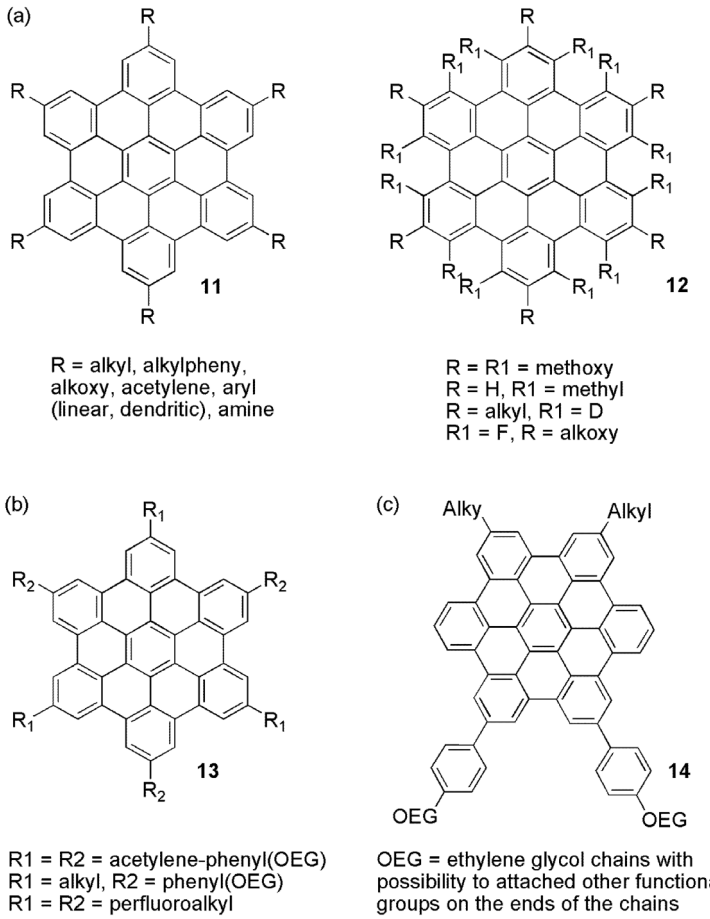


Fig. 1 Representative structures for functionalized HBC molecules. (a) Symmetrical 6-, 12-, and 18-fold-substituted HBCs; (b) Core-shell-type and (c) Gemini-shaped amphiphilic HBCs.

© 2012, IUPAC

Numerous novel HBC derivatives have been published in the past five years, opening a large range of applications for these discs-like molecules. Organogels can be prepared from amido-**15** and ureido **16** functionalized HBCs (Fig. 2) [51]. Pendant and ladder-type polymers containing HBC units have been reported with a polynorbornene backbone **17** [52]. Electron acceptor perylene monoimide was covalently attached to the HBC synthon through an acetylene linker via Sonogashira–Hagihara

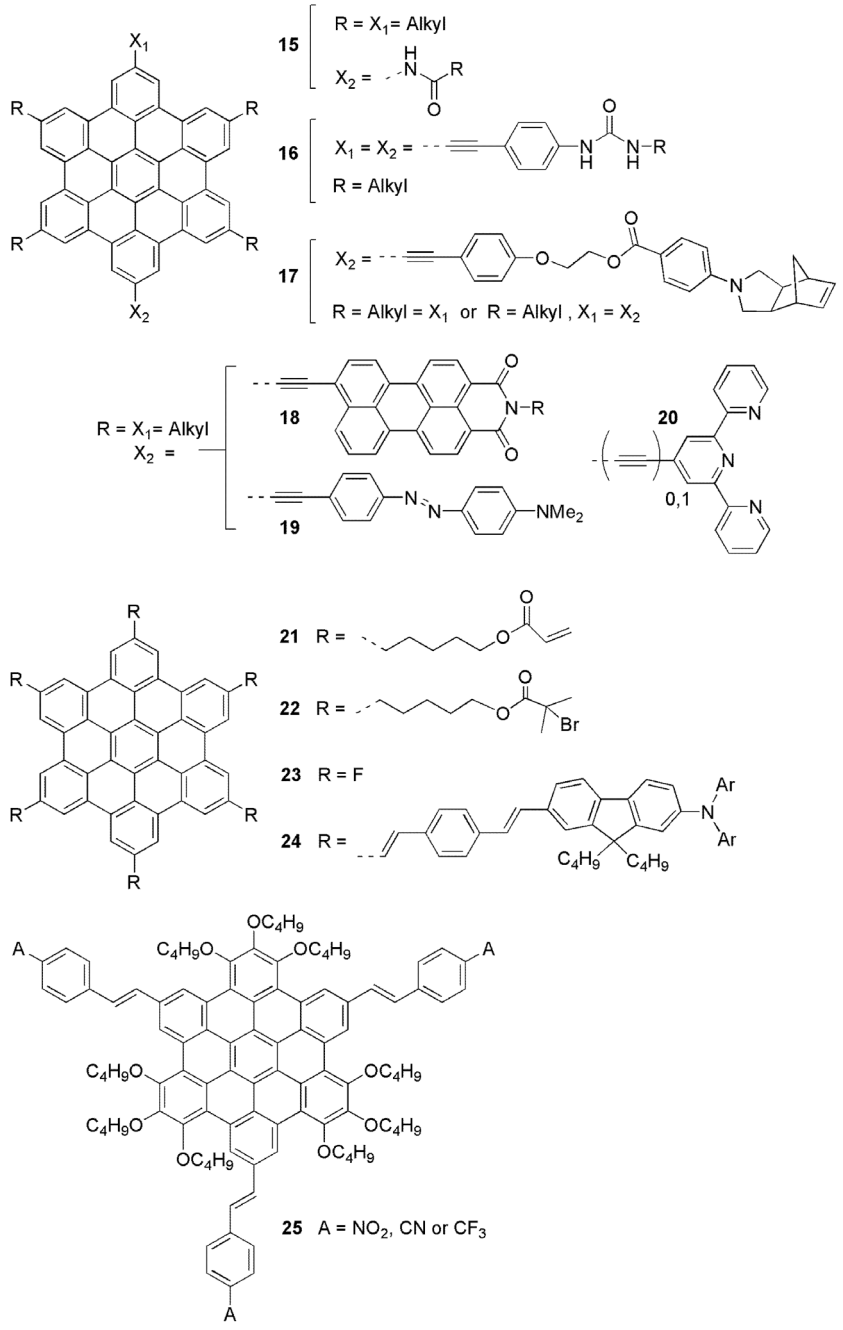


Fig. 2 Recently published HBCs with functional groups for hydrogen bonding, chemical cross-linking, optical absorption, and other applications.

cross-coupling from ethynyl-substituted HBC (Fig. 2, **18**) [53]. Similarly, an azobenzene moiety was anchored to the core to obtain an optical molecular switch **19** [54]. Terpyridine ligands have also been attached to the HBC core, leading to transition-metal complexes with HBC ligands **20** [29]. Stable columnar HBC structures have been achieved in high yield with acrylates **21** [55] or 2-bromo-2-methyl-propionic ester **22** [56] for physical cross-linking of the aggregates.

Unlike the synthesis of hexakis(iodo) HBC [11,25], Kikuzawa et al. reported the preparation of 2,5,8,11,14,17-hexafluoro-hexa-*peri*-hexabenzocoronene **23** via Diels–Alder route of 4,4'-difluoro-diphenylacetylene and tetrakis(4-fluorophenyl)cyclopentadienone. Subsequent Scholl-type transformation of the corresponding HPB either with $FeCl_3$ or $AlCl_3/Cu(OTf)_2$ afforded the product in moderate yields (47 and 64 %, respectively) [26]. The hexafluoro-substituents induce attractive intermolecular C–H···F–C interaction and reduce the energy of the frontier orbitals, resulting in n-type semiconductivity (vide infra) [57,58].

Star-shaped HBC **24** [59] and C3-symmertric "octupolar" HBC **25** [28] have been reported as attractive target molecules for two-photon absorption owing to their donor–acceptor characteristics. Six-fold symmetric compound **24** was prepared from the cyclized hexaiodo counterpart and subsequent attachment of the fully conjugated peripherial acceptors via Pd-catalyzed Heck reaction. Alternating donor and acceptor substituents in compound **25** were elegantly introduced starting with an asymmetric tolane carrying alkoxys and ester functionalities. From a triphosphonate HBC intermediate, nitro-, nitrile-, and trifluoromethyl were installed by Wittig–Wadsworth–Emmons reaction [28].

Soon after the first synthesis of the Gemini-shaped amphiphilic HBC derivatives **14** [34], a number of analogues with additional functionality and structural complexity emerged in the literature (Fig. 1c). HPBs (prepared via route 2 in Scheme 1 with symmetric or asymmetric alkynes) carrying photo-, electro-active units or halides for subsequent functionalization, were dehydrogenated under mild conditions in moderate to excellent yields. Some examples include coumarin [60], isothiouronium ion [61] tethers, electron acceptors 4,5,7-trinitro-9-fluorenone (TNF) [62], C_{60}-fullerenes [63], and dithienylethene pendants [50]. Reactive groups, such as thiols [64], norbonenes [65], azides [66], and pyridine [67], have also been appended to these amphiphilic HBCs. Various chemical transformations were performed to obtain stable peripherically functionalized conductive nanotubes.

Recently, a series of easily functionalized solution-processable fluorenyl HBC (FHBC) has been reported. HPBs carrying dioctylfluorenes were cyclized to give HBCs with the core structures **26–28** shown in Fig. 3 [68]. Reactive halide groups on the fluorene unit (Fig. 3, **29**) allowed diverse chemical transformations, such as lithium–halogen exchange, Suzuki–Miyaura cross-coupling, or Buchwald–Hartwig coupling. In this way, electron-donating arylamine **30** [27], thiophene **31** [69,70], porphyrin **32** [71], and fullerene **33** [72] derivatives were strategically synthesized.

© 2012, IUPAC

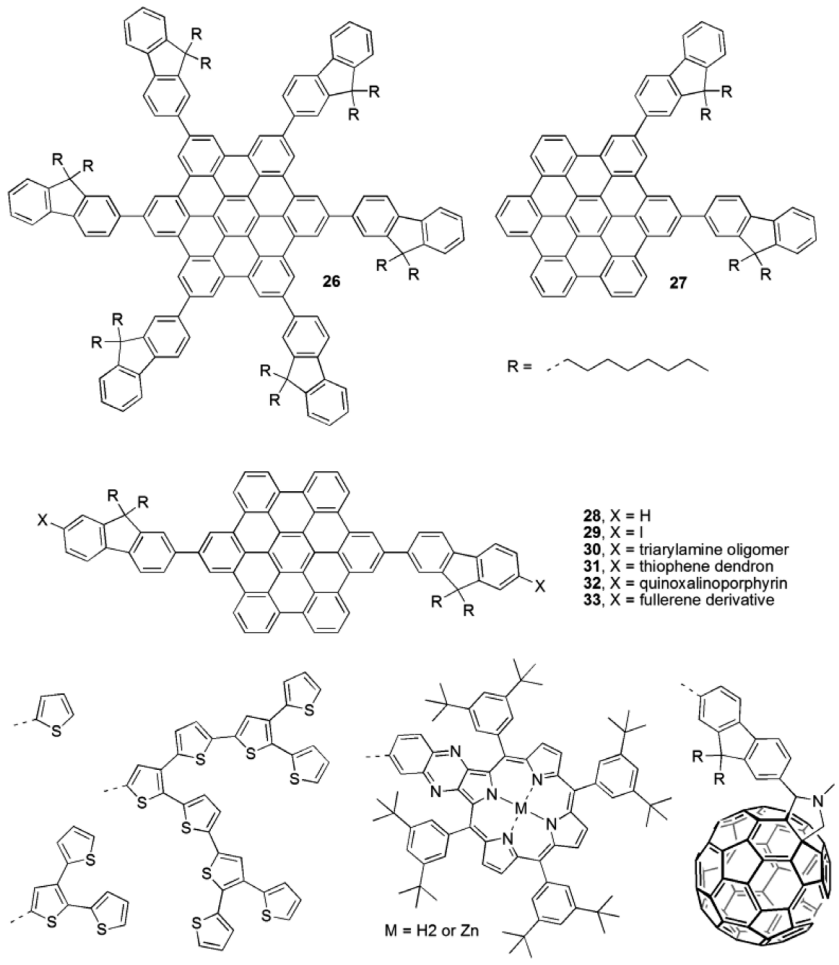


Fig. 3 FHBC core structure with pedant arylamines, thiophenes, porphyrins, and fullerenes.

PHYSICAL PROPERTIES AND MOLECULAR ORGANIZATION

Properties of PAHs are influenced by their molecular structure, size, and shape of the aromatic core. Depending on whether the rings are linearly fused (*cata* – fused) or angularly fused (*peri* – fused) leads to a wide variety of PAH with different shapes and size which in turn have pronounced effects on their physical as well as chemical properties. For example, molecules that are fused linearly have poor stability compared to their angularly fused homologues and tend to decompose via endoperoxide formation or dimerization [1,2]. This difference in their chemical reactivity and stability can be explained in terms of Clar's aromatic sextet (benzenoid character) rule which states that the larger the number of isolated aromatic sextets that can be drawn for a given structure the greater is the aromatic stabilization [73]. Another important effect of ring fusion in PAHs is on their crystal packing arrangements. Based on the relative orientation of the molecular planes in crystals, four different packing motifs are commonly encountered for PAH [74–76]. They are: (a) herringbone packing, where molecules have an edge-to-face interaction (e.g., anthracene); (b) sandwich herringbone packing, where a pair of π-stacked molecules have a herringbone interaction with another pair (e.g., pyrene); (c) γ motif, which is a flattened out herringbone (e.g., coronene); and (d) β motif, which is a layered structure made of graphitic planes (e.g., tribenzopyrene). The different packing arrangements arise as a result of the difference in

carbon to hydrogen atom ratios between the different structures, which in turn dictate whether C–H····π interactions or π–π interactions dominate in the solid state. Molecules with low C/H ratios are dominated by C–H····π interactions resulting in edge-to-face interactions, while high C/H ratios result in increased π–π interactions between the molecules as is the case with disc-shaped molecules like coronene. PAHs exhibiting either herringbone or π–π stacking interactions are expected to have high charge carrier mobilities and have been widely studied in the field of organic electronics [1,5].

The UV–vis spectrum of unsubstituted HBC in trichlorobenzene has been reported by Clar [77]. Similar to other PAHs, HBC exhibits three characteristic electronic absorption bands, namely, α, p, and β band based on the nomenclature introduced by Clar [78,79]. The α-band, which has the longest wavelength of the three characteristic bands, appears around 440 nm with low intensity and is attributed to the electronic transition from the second highest occupied molecular orbital (HOMO-1) to the lowest unoccupied molecular orbital (LUMO), also known as the 0–0 transition [80]. The p-band appears around 387 nm with moderate intensity and corresponds to a transition from HOMO to LUMO [80]. The β-band appears around a shorter wavelength of 360 nm with high intensity owing to the electronic transition from the HOMO to the second lowest unoccupied orbital (LUMO+1) [80]. Addition of both electron-donating and -withdrawing groups to the HBC core resulted in no significant change in the absorption profile. However, the addition of thiophene dendrimers to the HBC core via fluorene units leads to a modest bathochromic shift with a broader absorption [69]. While the symmetry of the substituted HBC core had very little effect on the absorption profile, the photoluminescence spectra of molecules with lower symmetry exhibited stronger 0–0 transition, which was weaker in HBC molecules with higher symmetry [81].

The single-crystal X-ray structure of unsubstituted HBC showed strong π–π interactions and packing in γ motif due to the high C/H ratio in the molecules (Fig. 4) [82,83]. The interplanar distance between the aromatic cores is 3.42 Å, which is slightly larger than that of graphite (3.35 Å). Owing to the close packing in the solid state, the molecules are tilted at an angle of 48º with respect to the basal plane (010). This tilt results in a center-to-center offset of 3.8 Å between the molecules within the π-stack. Another important aspect of HBC is that they are near planar, which is due to the decreased tendency of the bay regions to deviate from planarity, which can be attributed to long C–C bond distances observed at the central benzene ring. The fact that these molecules have large aromatic core enabling them to pack in a columnar stack with smaller interplanar distance makes them ideal candidates for charge transport layer in electronic devices.

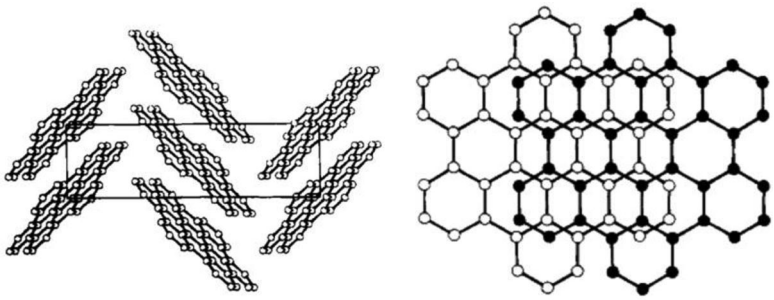


Fig. 4 Crystal structure of HBC **1** (adapted with permission from ref. [83], copyright © 1995 American Chemical Society).

While HBC exhibits better π-stacking in the solid state, it suffers from poor solubility, which is a key requirement in order to utilize low-cost solution-processing techniques. However, the progress in synthetic methodology has allowed the synthesis of novel HBC functionalized with solubilizing groups to address this issue. The nature and position of these groups can significantly influence their proper-

ties. For example, single-crystal X-ray diffraction (XRD) studies of permethoxylated HBC have shown that these molecules have nonplanar double-concave structure owing to steric interaction between the methoxy groups in the bay region [84].

Addition of longer solubilizing groups on the *peri* position of the outer phenyl rings maintained the planar structure and resulted in the segregation of the flexible side chains from the rigid aromatic core to give an insulated columnar arrangement [85,86]. A drawback of such an arrangement is that any defects within the stack can significantly affect their charge carrier mobility along the π-stacking direction (vide infra). The thermotropic behavior of substituted HBCs have been well studied using techniques such as differential scanning calorimetry (DSC) [81,87,88], solid-state NMR spectroscopy [89–91], polarized optical microscopy (POM) [81,87], and 2D wide-angle X-ray scattering (2D WAXS) [85]. While DSC is useful in determining the different phase transition present for a given molecule, 2D WAXS can provide more information on the packing arrangement at each phase. 2D WAXS studies have shown that the substituted HBC exhibits characteristic phase transition from the tilted columnar arrangement in the crystalline phase to the well-ordered liquid-crystalline phase where the molecular planes are stacked perpendicular to the columnar axis [92,93]. This behavior has allowed these molecules to self-heal by annealing at temperatures close to the phase transition temperature to give well-ordered structures. The chain length and degree of branching on the alkyl substituents have significant effects on melt or isotropization temperature. For example, HBC derivative with longer dodecyl chains has slightly lower isotropization temperature at 417 °C than the octyl-substituted derivative at 430 °C [87]. Further reduction in melt temperature has been achieved by using branched chain substituents [33,87,94]. This difference in melt behavior arises from the difference in the π–π interaction between the aromatic cores for different substituents.

In addition to their effect on solubility and melt temperature, substituents on the HBC core can also affect their aggregation in solution, thereby influencing their self-assembly and morphology of the resulting film [95]. Aggregation in solution has been studied using techniques such as ^{1}H NMR, UV–vis, and photoluminescence spectroscopy [95]. When bulky *t*-butyl substituent was used as the solubilizing group, no aggregation was observed owing to steric interactions. The longer linear dodecyl-substituted derivative exhibited self-aggregation in solution and existed as a monomer at concentration lower than 10^{-6} M in 1,1,2,2-tetrachloroethane-d_2 determined using ^{1}H NMR study. Branched alkyl substituents had a significant effect on aggregation from solution with longer dovetail chain substituents exhibiting poor aggregation than the shorter branch owing to the steric interaction with the aromatic core. FHBC derivatives aggregated strongly in solution [68–72]. It is clear from concentration-dependent ^{1}H NMR studies that 2,11-FHBC derivatives π–π stack strongly on the HBC core [68]. However, the HBC discs are thought to be arranged in a staggered manner within the columnar stacks owing to the steric bulk of the fluorene units. Addition of other substituents on these FHBC derivatives has led to helical packing arrangement as well as a switch from columnar to lamellar packing in solid state [69,70]. The influence of substituents on molecular self-assembly has important consequences for devices containing these functional materials (vide infra).

Asymmetrical HBCs with carboxylic acid group at the alkyl chain termini were synthesized to take advantage of hydrogen-bonding interaction in the solid state to stabilize the columnar arrangement [88]. Monocarboxylic acid functionalized HBC self-assembled into dimers owing to hydrogen-bonding interactions with carboxylic acid groups of neighboring HBC molecules, resulting in a closely packed hexagonal arrangement without any tilting between the columns. Increasing the length of the alkyl tether connecting the carboxylic acid group to the HBC core disrupted the hydrogen-bonding interaction, resulting in a tilted columnar arrangement indicating the steric requirements imposed by the longer tether. Addition of another carboxylic acid group *para* to monocarboxylic acid further enhanced the supramolecular stability by hydrogen-bonded polymer formation, resulting in an oblique arrangement with no tilting between the columnar stacks.

The family of Gemini-shaped amphiphilic HBC derivatives exhibited distinct self-assembly behavior compared to other HBC systems (Fig. 5) [34,50,60–67,96–101]. Owing to the vast difference

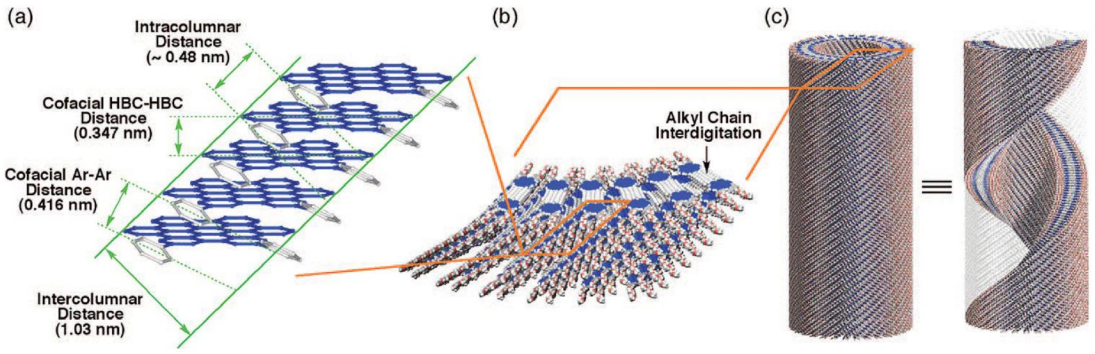


Fig. 5 Schematic representation of packing arrangements in nanotubes (reprinted with permission from ref. [97], copyright © 2008 American Chemical Society).

in the side-chain properties, these molecules formed bilayers in solution in which the alkyl chains of the two HBC layers were interdigitated, forming a closely packed structure leaving the hydrophilic side chains exposed on the outside. This 2D pseudo-graphite tape containing π-stacked amphiphilic HBC molecules eventually self-assembled to form nanotubes that were characterized by scanning electron microscopy (SEM). HBC core in this tubular arrangement π-stacked along the long axis of the tube with an interplanar distance of 3.6 Å. The tubular arrangement was thermally stable, however, heating it to higher temperature led to disruption of the tubular arrangement.

A systematic study showed that the lipophilic side chains along with phenyl substituents were absolutely essential for the nanotube formation [97]. While the hydrophilic tetraethylene glycol (TEG) chains on the phenyl substituents were not necessary for the tubular arrangement, they do promote the slow self-assembly in solution by improving solubility. 2D WAXS studies showed that the π-stacked HBC units were tilted by 45º relative to the long axis of the column with an interplanar spacing of 3.47 Å (Fig. 3). The 45º tilt causes a center-to-center offset of 4.8 Å between the HBC core, resulting in the formation of a coiled structure in order to prevent steric congestion between the phenyl rings. Depending on the chiral nature of the substituents on the phenyl ring, they can tilt either clockwise or anti-clockwise relative to the HBC core, which in turn determines the helical chirality of the resulting nanotube [96,99,100].

Depending on the way HBC columnar aggregates in solution assemble on substrates, two different arrangements are possible (Fig. 6). "Edge-on", or homogeneous alignment, refers to the π-stacking direction parallel to the substrate and "face-on", or homeotropic arrangement, refers to the columnar π-stacking direction perpendicular to the substrate (Fig. 2). In most cases, the edge-on arrangement is

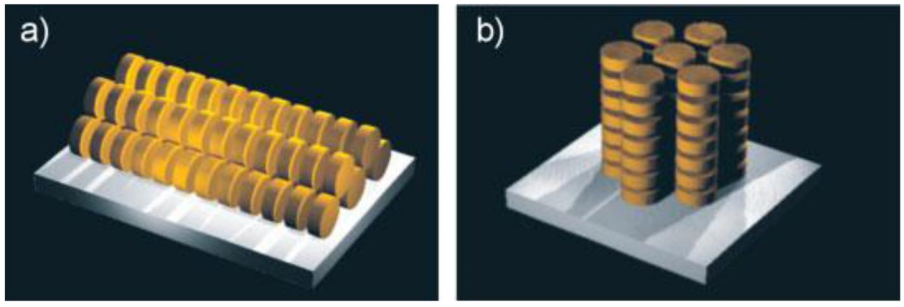


Fig. 6 Schematic representation of possible orientation on substrates (a) edge-on orientation (b) face-on orientation (reprinted with permission from ref. [94], copyright © 2005 John Wiley).

preferred for HBC derivatives. However, substituents on the HBC core can play a role in the molecular ordering on substrates. HBC with tetramethylhexadecyl (HBC-$C_{4,16}$) substituents were shown to exhibit homeotropic ordering in films deposited between two indium tin oxide (ITO) substrates [87]. Photoconductivity measurements on films deposited between ITO substrates exhibited high short-circuit current at regions where the molecules stacked with a face-on arrangement compared to regions where the molecules stacked with an edge-on arrangement as evidenced by POM. HBC molecules with branched alkoxy substituents also exhibited face-on arrangement in films sandwiched between two substrates [94].

Molecular arrangement, especially longer-range order, can be controlled using a variety of processing techniques. Molecular ordering of amphiphilic HBC molecules on different substrates have been achieved using Langmuir–Blodgett (LB) technique. Films of amphiphilic HBC with branched hydrophilic chains exhibited face-on arrangement when deposited on solid substrates using LB technique [33]. The unique orientation is not only due to the hydrophilic nature of the oligoether substituents (HBC), which allows it to be submerged in the water phase, but also to the branched substituents, which prevent edge-on orientation. LB films made from unsymmetrical HBC containing carboxylic acid terminated alkyl chain (HBC) also formed well-ordered films with an edge-on orientation [102]. Two different crystalline phases were observed on the substrate depending on the pressure applied during the film deposition. In the high-pressure phase, the alkyl chains were closely packed resulting in increased interplanar spacing between the HBC core, while in the low-pressure phase the alkyl chains are disordered, however, the HBC core is tightly packed together resulting in lower HOMO–LUMO gaps compared to the high-pressure phase.

Solid-state samples prepared by extrusion of neat materials showed some interesting behavior of HBC derivatives under macroscopic alignment. Typically, for symmetric disc-shaped HBC derivatives, the self-assembled HBC columnar structures tend to align in the direction of the extrusion (Fig. 7) [85]. There is a recent report on the nanostructuring of HBC films by an imprinting technique using anodized aluminum oxide [103]. Exact pattern transfer of nanoscale columns was achieved using a HBC derivative with cross-linkable acrylate groups. HBC derivatives have also been directionally aligned on surfaces using techniques such as zone casting, magnetic alignment, and deposition on structured surfaces. These studies will be discussed in more detail in the next section, and macroscopic alignment of molecules can have major effects on device performance of bulk materials.

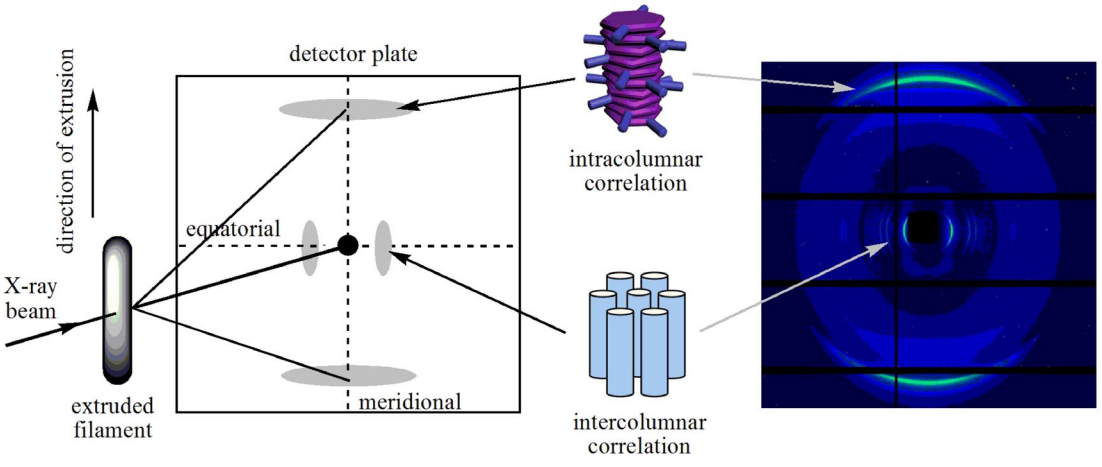


Fig. 7 Schematic representation of the experimental set-up (left) and a characteristic 2D WAXS pattern of HBC derivative **28** (right) showing intra- and intercolumnar organization.

HBCs AS FUNCTIONAL MATERIALS

Having discussed the synthesis and self-assembly of HBC derivatives, the third section of this article will focus on HBCs as functional materials. HBC and most of its derivatives exhibit strong π–π stacking leading to self-assembled structures with long-range order. This is the primary feature that is the basis of functional materials constructed from the HBC core molecule.

A number of functional materials have been reported by taking advantage of the long-range structural order of HBC derivatives. Lithium-ion battery materials development is one area that has received some interest [104,105]. It has been reported that HBC films can store high levels of lithium and sodium, with up to one alkali metal atom to four carbon atoms, in photoelectron spectroscopic studies [104]. More recently, the electrochemical behavior of unsubstituted HBC and its hexafluoro derivative **23** in nonaqueous lithium cell medium was reported [105]. Discharge capacity as high as 460 and 1230 mAh/g was measured for HBC and 6F-HBC, respectively, indicating potential use of these materials as the negative electrode in lithium-ion batteries. As mentioned in the synthesis section, HBC derivatives have also been used as synthetic precursors to form other nanostructured materials [106,107]. In a recent report, the HBC-C12 derivative was used to create nanostructured hollow spheres [108]. High reversible capacity (ca. 600 mAh/g) and excellent high-rate capability (about 200 mAh/g at the rate of 10 °C) were achieved when these hollow carbon spheres were used as anode material for lithium-ion batteries.

Owing to the incompatibility of typical HBC derivatives with aqueous medium, few functional HBC materials for biological applications have been reported. In one study, a HBC chromophore **24** capable of two-photon absorption was incorporated into phospholipid-polyethyleneglycol micelles [59]. With the addition of magnetic nanoparticles in the micelles, magnetically guided two-photon cell imaging was achieved. Water-solubilized HBC derivatives with carboxylate groups have been reported [56]. These negatively charged HBC nanofiber assemblies associated strongly with positively charged peptides and could pave the way for biological sensing applications. HBC derivatives have been used in OFET sensor devices for volatile organic compounds [109,110]. In these sensors, carbon nanotubes are the electroactive material in the device with the HBC derivative used as a surface coating to modulate sensitivity and selectivity.

Perhaps the most obvious function of HBCs is as semiconducting materials [111]. The π–π stacked columnar structure of HBC means that its intrinsic charge mobility can be very high, up to 1.1 cm^2/Vs [112]. This has led to a range of applications in organic electronics such as OFETs and organic photovoltaics (OPVs). The most interesting and recent HBC-based organic electronic devices will be highlighted in the following section.

The charged transport of HBC materials has been the topic of investigation in many papers. While the local intracolumnar charge transport for HBC has been examined using pulse-radiolysis time-resolved microwave conductivity (PR-TRMC) measurements [112–115], bulk charge transport is of greater interest to organic electronic applications. Perhaps the most convenient device for obtaining charge mobility of bulk materials is OFETs. Depending on substituents on the HBC core and OFET fabrication methods, charge mobility can range from 10^{-6} to 10^{-2} cm^2/Vs [116–122]. Films of unsubstituted HBC have been obtained by vacuum deposition and hole mobility of 3.3×10^{-2} cm^2/Vs has been measured [122]. XRD measurements of these films indicate a herringbone packing of the HBC molecules with the plane of the HBC "edge-on" to the substrate surface. Molecular alignment is a key parameter in determining OFET mobility. For HBC films containing 1D columnar structures, anisotropy in charge mobility can be high. This phenomenon has been observed for a range of solution-processable alkyl-substituted HBC derivatives. Aligned films of alkyl-substituted HBCs have been fabricated by deposition on oriented substrates [116], by magnetic alignment [118], and by solution-processing techniques such as zone casting [121]. Both films aligned on friction-oriented poly(tetrafluoroethylene) and by magnetic forces gave hole mobility in the 10^{-3} cm^2/Vs range if the direction of the HBC columns is aligned from the source to the drain electrodes of the OFET device [116,118]. For devices where the

© 2012, IUPAC

HBC columns were aligned in the same direction as the OFET channel, the mobility drops to below 10^{-5} cm^2/Vs. The highest solution-processed OFET mobility report is 10^{-2} cm^2/Vs for zone-casted HBC films [121]. From XRD and TEM measurements, HBC columns are lying parallel to the substrate with long-range order in one direction (Fig. 8). With defects in the aligned film, mobility of 10^{-2} cm^2/Vs is still two orders of magnitude lower than the intrinsic intracolumn mobility. Isotropic films of alkyl-substituted HBCs, deposited by spin coating, showed mobilities below 10^{-5} cm^2/Vs. Interestingly, a 9,9-dioctylfluorene-substituted HBC derivative gave OFET mobility in the 10^{-3} cm^2/Vs range [68]. This solution-processable HBC was deposited by spin coating, and alignment techniques were not applied. In fact, it is clear from thin film XRD experiments that HBC columnar structures were present in the films with no long-range directional order. The most likely reason for the OFET performance difference between alkyl- and fluorene-substituted HBC films is the positioning of the solubilizing alkyl chains on these materials. Essentially, assembled columns of alkyl-substituted HBCs are analogous to insulated wires. Although it has been shown that electron tunnelling through the lipophilic alkyl layer is possible [123], this still represents a significant barrier for intercolumn charge mobility. Charge mobility in fluorene-substituted HBCs is not affected by solubilizing alkyl chains. It is possible that charges are able to hop easily between columns via the fluorene group. The fact that unsubstituted HBC films with no special alignment also showed OFET mobility in the 10^{-2} cm^2/Vs range supports this hypothesis [122]. Perhaps aligned films of fluorene-substituted HBCs or unsubstituted HBC will give charge mobility closer to the intrinsic intracolumn value obtained by PR-TRMC.

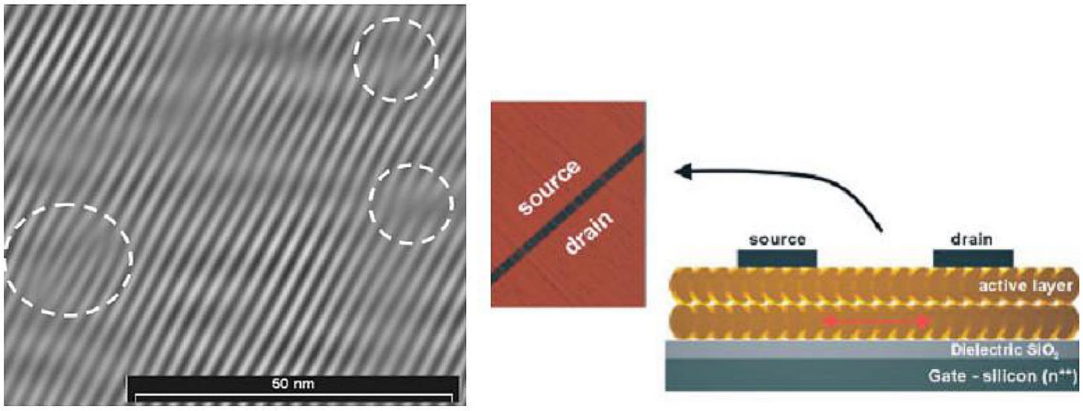


Fig. 8 Aligned HBC films fabricated using zone casting technique for OFET application (adapted with permission from ref. [121], copyright © 2005 John Wiley).

From frontier molecular orbital and charge mobility measurements, it is clear that the unsubstituted HBC core is a hole transport material. Nevertheless, chemical modification of the core molecule can lead to electron-transport materials. The hexafluoro-HBC **23** is an electron-transport material (Fig. 2) [58]. In evaporated OFET devices, electron mobility of 1.6×10^{-2} cm^2/Vs has been reported. Interestingly, the crystal orientation of the evaporated films showed face-to-face packing of the HBC molecules with the planes of the HBC perpendicular to the substrate surface. This molecular arrangement is ideal for OFET devices, and performance could be further improved if the HBC columnar stacks and crystallites can be directionally aligned. The charge mobility of another fluorinated HBC **12**, where R = alkoxy and R1 = F, has been measured by PR-TRMC, giving a value of 2.8×10^{-2} cm^2/Vs (Fig. 1) [124]. Although frontier orbital measurements suggest higher electron affinity for this material compared to the nonfluorinated derivative, hole and electron mobilities cannot be distinguished in PR-TRMC measurements.

© 2012, IUPAC

Ambipolar behavior has also been observed in HBC derivatives. HBC compounds appended with the electron-accepting perylene monoimide have been reported (Fig. 2, **18**) [53,125]. High structural order was observed ranging from molecular monolayers on surfaces to macroscopic fibers through electron microscopy and X-ray experiments. Nanocrystalline films gave OFET mobility of 7×10^{-5} and 1×10^{-4} cm^2/Vs for electrons and holes, respectively [53]. HBC-fullerene hybrid materials have also been reported in the literature [63,72]. Ambipolar OFET behavior was observed for these systems with electron and hole mobilities ranging from 10^{-5} to 10^{-7} cm^2/Vs. The primary interest in these HBC-fullerene materials is in photocurrent generation, which will be discussed in more detail in the following OPV section. It should be mentioned here that other techniques, apart from OFET and PR-TRMC, can be used to measured charge mobility in HBC materials. These include space-charge limited-current (SCLC) technique [126] and photogenerated charge measurements such as time-of-flight (TOF) [127,128] and charge extraction by linearly increasing voltage (CELIV) [129].

HBC derivatives have been materials of interest for OPV applications. Early reports showed combinations of electron-donating alkyl-substituted HBCs with electron-accepting perylene diimides (PDIs) [130,131]. The initial report on the HBC-PDI blend system showed a degree of phase separation between the HBC and PDI components in solution-deposited films with PDI crystallites extending from the top surface of the films [131]. A maximum external quantum efficiency (EQE) of 34 % was recorded at 490 nm, and the power conversion efficiency (PCE) was 1.95 % measured at the same wavelength with very low intensity light (0.47 mW/cm^2). Owing to the low illumination intensity used, it should be noted here that the efficiency numbers quoted in this early work cannot be compared directly with more recent state-of-the-art results measured using high-intensity (100 mW/cm^2) solar-simulated light source. Although the device performance is orders of magnitude lower than the current state-of-the-art bulk heterojunction (BHJ) devices, this is the first demonstration of photovoltaic effect in discotic electron donor and acceptor blend materials. Subsequent studies using different alkyl HBC and PDI derivatives gave only modest improvements in performance [132]

A substantial improvement in OPV performance was obtained for HBC materials substituted with solubilizing fluorene units (Fig. 9) [68]. In combination with the electron-accepting fullerene derivative ($PC_{61}BM$), BHJ photovoltaic cells were fabricated and gave high open-circuit voltage of 0.9 V and PCE of 1.5 % under simulated AM 1.5 G illumination conditions (Fig. 9d). This is remarkable given that fact that the HBC/$PC_{61}BM$ blend film only captures a fraction of the solar spectrum with their limited absorption range [68]. Even more intriguing is the high fill factor of up to 65 % for these BHJ devices. Fill factor characteristic of a BHJ device is typically an indication of blend morphology and charge transport efficiency. In atomic force microscopy and X-ray experiments, it was clear that the electron donor and acceptor phases separated into ideal nanoscale domains with retention of HBC columnar structures in the electron donor phase (Figs. 9b,c). This meant there was a high interfacial area for charge separation and charge transport was efficient within the donor and acceptor phases. As discussed in the previous section on OFETs, these fluorine-substituted HBCs showed good hole mobility without applying special molecular alignment techniques. Interestingly, the OFET mobility of FHBC/$PC_{61}BM$ blends gave balanced hole and electron mobility in the 10^{-4} cm^2/Vs range [68]. This corresponds well with the OPV device characteristics.

With such encouraging devices, efforts were made to improve the spectral absorption of these fluorine-substituted HBC materials. Chromophores with a range of photophysical properties were attached to the FHBC core material including triarylamine oligomers, oligothiophenes, porphyrins, and organic dyes [27,69–71]. In the best oligothiophene-HBC system, PCE as high as 3 % was obtained in combination with the $PC_{71}BM$ acceptor [69,70]. A clear correlation between molecular structure and device performance emerged from these studies. While the addition of chromophores improved spectral absorption of these materials, the size and shape of the substituents had a major influence on donor–acceptor blend morphology. In the case of the dendritic oligothiophene derivatives, large dendron size changed the solid-state molecular aggregation of the material leading to a drop in charge transport efficiency [70]. FHBC-fullerene derivatives were also tested as a single-component material in

© 2012, IUPAC

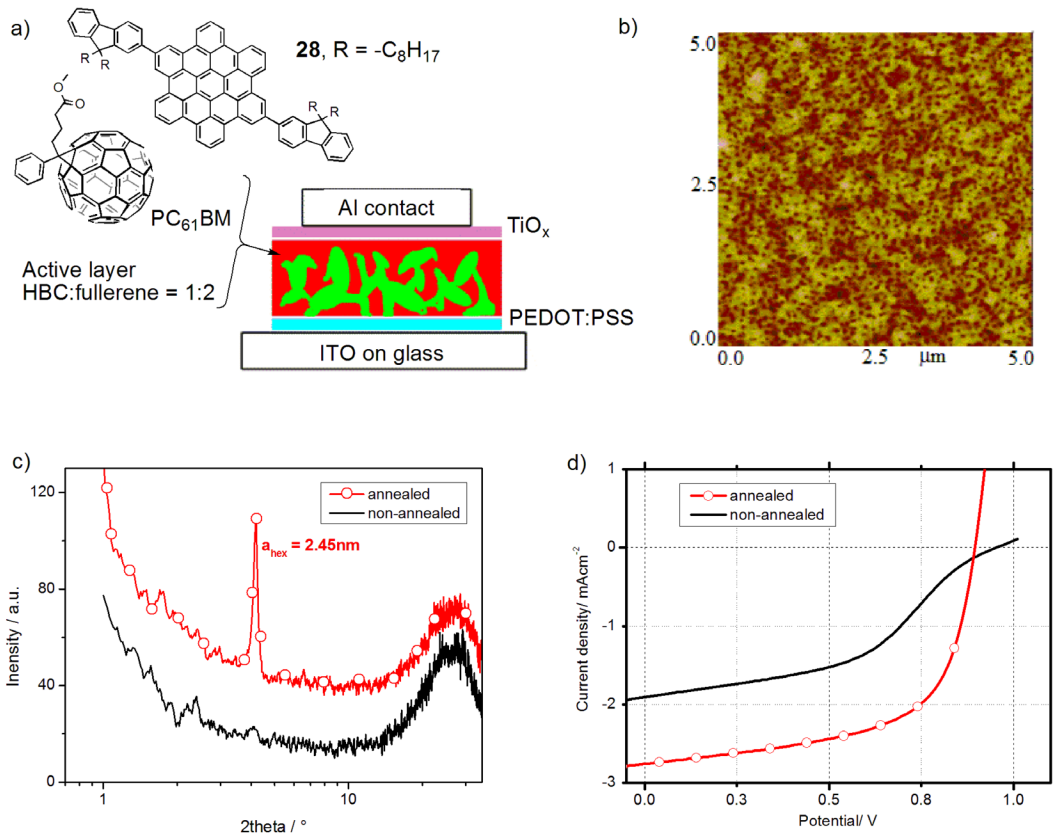


Fig. 9 (a) Illustration of solar cell device structure with a blend of HBC derivative **28** and $PC_{61}BM$ (1:2) as the active layer. (b) Atomic force microscopy (AFM) topographic image of the blend film showing phase separation. (c) Thin film X-ray scattering of the blend film before and after annealing. (d) Current–voltage curves of the solar cell device before and after annealing.

OPV devices [72]. With electron donor and acceptor on the same molecule, no blending was required. Remarkably, there was evidence of self-assembled HBC columnar structures despite covalent attachment of the bulky fullerene moiety to the HBC core. A maximum PCE of 0.25 % was recorded for the single-component OPV devices. One problem with these FHBC-fullerene compounds is the short distance between the donor and acceptor units. One of the major loss mechanisms in device efficiency is thought to be charge recombination [72].

Carbon nanotube structures based on amphiphilic HBC derivatives have also been applied to organic electronic devices [50,62,63,98]. The unique nanotubular arrangement of amphiphilic HBCs along with their ability to form radical cations on oxidation opens up their application in optoelectronic devices. Nanotubes formed from TNF-appended amphiphilic HBC exhibited photochemical generation of charge carriers measured using micrometer gap electrodes on a silicon substrate [62,98]. In line with other HBC derivatives, amphipilic HBCs also showed hole-transporting properties in OFETs. HBC nanotube assemblies with fullerenes appended to the periphery of the nanotubes have been reported [63]. The bulky fullerene substituents did not hinder the self-assembly process and indeed enhanced the nanotube formation by fullerene aggregation. The nanotubes exhibited ambipolar behavior with electron and hole mobility of 1.1×10^{-5} and 9.7×10^{-7} cm^2/Vs. In order to measure the intrinsic hole mobility within the tubes, PR-TRMC measurement was performed on nanotubes yielding a hole mobility of 2 cm^2/Vs. Since OPV measurements using conventional device architecture gave shorted devices with

pin holes, side electrode configuration using PEDOT:PSS/Au/Ti and TiO_x/Ti/Al as electrodes was used. The maximum EQE obtained at 360 nm was 2 %. Even though these amphiphilic HBC systems can give well-ordered structures in the nm to micron range, the low OPV device performance is an indication that huge challenges still remain in the control of bulk and interfacial material properties.

SUMMARY AND FUTURE DIRECTIONS

HBC remains a molecule of interest owing to its unique properties, particularly in molecular organization and charge transport. The synthetic tools for HBC and its derivatives are very well developed, and the variety of functional groups that is possible on the HBC molecule is virtually limitless. In addition, more convenient methods to achieve the HBC core have enabled production of materials in the multigram scale. HBC derivatives have been employed as functional materials in a range of applications from sensors and batteries to transistors and solar cells. Control of molecular self-assembly is essential in most applications. While the use of functional groups and various processing techniques have led to well-ordered and aligned bulk materials as well as intricate carbon nanotube assemblies, much research is still required to tailor bulk material properties to specific applications through design of molecules and control of their organization.

REFERENCES

1. J. E. Anthony. *Angew. Chem., Int. Ed.* **47**, 452 (2008).
2. J. E. Anthony. *Chem. Rev.* **106**, 5028 (2006).
3. D. J. Gundlach, J. E. Royer, S. K. Park, S. Subramanian, O. D. Jurchescu, B. H. Hamadani, A. J. Moad, R. J. Kline, L. C. Teague, O. Kirillov, C. A. Richter, J. G. Kushmerick, L. J. Richter, S. R. Parkin, T. N. Jackson, J. E. Anthony. *Nat. Mater.* **7**, 216 (2008).
4. S. K. Park, T. N. Jackson, J. E. Anthony, D. A. Mourey. *Appl. Phys. Lett.* **91**, 063514 (2007).
5. J. Wu, W. Pisula, K. Müllen. *Chem. Rev.* **107**, 718 (2007).
6. E. Clar, C. T. Ironside. *Proc. Chem. Soc.* 150 (1958).
7. A. Stabel, P. Herwig, K. Müllen, J. P. Rabe. *Angew. Chem., Int. Ed.* **34**, 1609 (1995).
8. C. Kübel, K. Eckhardt, V. Enkelmann, G. Wegner, K. Müllen. *J. Mater. Chem.* **10**, 879 (2000).
9. K. P. C. Vollhardt. *Angew. Chem.* **96**, 525 (1984).
10. K. P. C. Vollhardt. *Acc. Chem. Res.* **10**, 1 (1977).
11. J. A. Hyatt. *Org. Prep. Proced. Int.* **23**, 460 (1991).
12. X. L. Feng, W. Pisula, L. J. Zhi, M. Takase, K. Müllen. *Angew. Chem., Int. Ed.* **47**, 1703 (2008).
13. X. Feng, W. Pisula, M. Takase, X. Dou, V. Enkelmann, M. Wagner, N. Ding, K. Müllen. *Chem. Mater.* **20**, 2872 (2008).
14. S. Ito, M. Wehmeier, J. Dietrich Brand, C. Kübel, R. Epsch, J. P. Rabe, K. Müllen. *Chem.—Eur. J.* **6**, 4327 (2000).
15. A. Fechtenkötter, N. Tchebotareva, M. D. Watson, K. Müllen. *Tetrahedron* **57**, 3769 (2001).
16. X. Yang, X. Dou, K. Müllen. *Chem. Asian J.* **3**, 759 (2008).
17. J. Wu, M. Baumgarten, G. Debije Michael, M. Warman John, K. Müllen. *Angew. Chem., Int. Ed.* **43**, 5331 (2004).
18. S. H. Wadumethrige, R. Rathore. *Org. Lett.* **10**, 5139 (2008).
19. X. Feng, J. Wu, V. Enkelmann, K. Müllen. *Org. Lett.* **8**, 1145 (2006).
20. R. Scholl, J. Mansfeld. *Ber. Dtsch. Chem. Ges.* **43**, 1734 (1910).
21. P. Kovacic, M. B. Jones. *Chem. Rev.* **87**, 357 (1987).
22. M. Müller, C. Kübel, K. Müllen. *Chem.—Eur. J.* **4**, 2099 (1998).
23. L. Y. Zhai, R. Shukla, R. Rathore. *Org. Lett.* **11**, 3474 (2009).
24. P. Rempala, J. Kroulík, B. T. King. *J. Org. Chem.* **71**, 5067 (2006).
25. J. Wu, M. D. Watson, K. Müllen. *Angew. Chem., Int. Ed.* **42**, 5329 (2003).

© 2012, IUPAC

26. Y. Kikuzawa, T. Mori, H. Takeuchi. *Org. Lett.* **9**, 4817 (2007).
27. W. W. H. Wong, D. J. Jones, C. Yan, S. E. Watkins, S. King, S. A. Haque, X. M. Wen, K. P. Ghiggino, A. B. Holmes. *Org. Lett.* **11**, 975 (2009).
28. Z. Zeng, Z. Guan, Q.-H. Xu, J. Wu. *Chem.—Eur. J.* **17**, 3837 (2011).
29. F. A. Murphy, S. M. Draper. *J. Org. Chem.* **75**, 1862 (2010).
30. X. Feng, W. Pisula, M. Ai, S. Groeper, J. P. Rabe, K. Müllen. *Chem. Mater.* **20**, 1191 (2008).
31. X. Dou, X. Yang, G. J. Bodwell, M. Wagner, V. Enkelmann, K. Müllen. *Org. Lett.* **9**, 2485 (2007).
32. K. Weiss, G. Beernink, F. Dotz, A. Birkner, K. Müllen, C. H. Woll. *Angew. Chem., Int. Ed.* **38**, 3748 (1999).
33. M. Lee, J.-W. Kim, S. Peleshanko, K. Larson, Y.-S. Yoo, D. Vaknin, S. Markutsya, V. V. Tsukruk. *J. Am. Chem. Soc.* **124**, 9121 (2002).
34. J. P. Hill, W. Jin, A. Kosaka, T. Fukushima, H. Ichihara, T. Shimomura, K. Ito, T. Hashizume, N. Ishii, T. Aida. *Science* **304**, 1481 (2004).
35. Y. Y. Lu, J. S. Moore. *Tetrahedron Lett.* **50**, 4071 (2009).
36. X. Feng, W. Pisula, T. Kudernac, D. Wu, L. Zhi, S. De Feyter, K. Müllen. *J. Am. Chem. Soc.* **131**, 4439 (2009).
37. J. Wu, M. D. Watson, L. Zhang, Z. Wang, K. Müllen. *J. Am. Chem. Soc.* **126**, 177 (2004).
38. S. K. Sadhukhan, C. Viala, A. Gourdon. *Synthesis* 1521 (2003).
39. P. T. Herwig, V. Enkelmann, O. Schmelz, K. Müllen. *Chem.—Eur. J.* **6**, 1834 (2000).
40. O. F. Aebischer, P. Tondo, B. Alameddine, T. A. Jenny. *Synthesis* 2891 (2006).
41. B. Alameddine, O. F. Aebischer, W. Amrein, B. Donnio, R. Deschenaux, D. Guillon, C. Savary, D. Scanu, O. Scheidegger, T. A. Jenny. *Chem. Mater.* **17**, 4798 (2005).
42. L. Zhai, R. Shukla, S. H. Wadumethrige, R. Rathore. *J. Org. Chem.* **75**, 4748 (2010).
43. A. A. O. Sarhan, C. Bolm. *Chem. Soc. Rev.* **38**, 2730 (2009).
44. B. T. King, J. Kroulik, C. R. Robertson, P. Rempala, C. L. Hilton, J. D. Korinek, L. M. Gortari. *J. Org. Chem.* **72**, 2279 (2007).
45. P. Rempala, J. Kroulík, B. T. King. *J. Am. Chem. Soc.* **126**, 15002 (2004).
46. M. Di Stefano, F. Negri, P. Carbone, K. Müllen. *Chem. Phys.* **314**, 85 (2005).
47. A. J. Berresheim, M. Müller, K. Müllen. *Chem. Rev.* **99**, 1747 (1999).
48. S. Laschat, A. Baro, N. Steinke, F. Giesselmann, C. Hägele, G. Scalia, R. Judele, E. Kapatsina, S. Sauer, A. Schreivogel, M. Tosoni. *Angew. Chem., Int. Ed.* **46**, 4832 (2007).
49. S. Sergeyev, W. Pisula, Y. H. Geerts. *Chem. Soc. Rev.* **36**, 1902 (2007).
50. Y. He, Y. Yamamoto, W. Jin, T. Fukushima, A. Saeki, S. Seki, N. Ishii, T. Aida. *Adv. Mater.* **22**, 829 (2010).
51. X. Dou, W. Pisula, J. Wu, G. J. Bodwell, K. Müllen. *Chem.—Eur. J.* **14**, 240 (2008).
52. C.-W. Chen, H.-Y. Chang, S.-L. Lee, I. J. Hsu, J.-J. Lee, C.-h. Chen, T.-Y. Luh. *Macromolecules* **43**, 8741 (2010).
53. J. M. Mativetsky, M. Kastler, R. C. Savage, D. Gentilini, M. Palma, W. Pisula, K. Müllen, P. Samori. *Adv. Funct. Mater.* **19**, 2486 (2009).
54. M. Ai, S. Groeper, W. Zhuang, X. Dou, X. Feng, K. Müllen, J. Rabe. *Appl. Phys. A* **93**, 277 (2008).
55. M. Kastler, W. Pisula, R. J. Davies, T. Gorelik, U. Kolb, K. Müllen. *Small* **3**, 1438 (2007).
56. M. Z. Yin, J. Shen, W. Pisula, M. H. Liang, L. J. Zhi, K. Müllen. *J. Am. Chem. Soc.* **131**, 14618 (2009).
57. S. Entani, T. Kaji, S. Ikeda, T. Mori, Y. Kikuzawa, H. Takeuchi, K. Saiki. *J. Phys. Chem. C* **113**, 6202 (2009).
58. T. Mori, Y. Kikuzawa, H. Takeuchi. *Org. Electron.* **9**, 328 (2008).
59. Q. Zheng, T. Y. Ohulchanskyy, Y. Sahoo, P. N. Prasad. *J. Phys. Chem. C* **111**, 16846 (2007).
60. J. Motoyanagi, T. Fukushima, N. Ishii, T. Aida. *J. Am. Chem. Soc.* **128**, 4220 (2006).
61. G. Zhang, W. Jin, T. Fukushima, A. Kosaka, N. Ishii, T. Aida. *J. Am. Chem. Soc.* **129**, 719 (2007).

© 2012, IUPAC

62. Y. Yamamoto, T. Fukushima, A. Saeki, S. Seki, S. Tagawa, N. Ishii, T. Aida. *J. Am. Chem. Soc.* **129**, 9276 (2007).
63. Y. Yamamoto, G. X. Zhang, W. S. Jin, T. Fukushima, N. Ishii, A. Saeki, S. Seki, S. Tagawa, T. Minari, K. Tsukagoshi, T. Aida. *Proc. Natl. Acad. Sci. USA* **106**, 21051 (2009).
64. J. Motoyanagi, T. Fukushima, A. Kosaka, N. Ishii, T. Aida. *J. Polym. Sci., Part A: Polym. Chem.* **44**, 5120 (2006).
65. T. Yamamoto, T. Fukushima, Y. Yamamoto, A. Kosaka, W. Jin, N. Ishii, T. Aida. *J. Am. Chem. Soc.* **128**, 14337 (2006).
66. J. L. Mynar, T. Yamamoto, A. Kosaka, T. Fukushima, N. Ishii, T. Aida. *J. Am. Chem. Soc.* **130**, 1530 (2008).
67. W. Zhang, W. S. Jin, T. Fukushima, N. Ishii, T. Aida. *Angew. Chem., Int. Ed.* **48**, 4747 (2009).
68. W. W. H. Wong, T. B. Singh, D. Vak, W. Pisula, C. Yan, X. L. Feng, E. L. Williams, K. L. Chan, Q. Mao, D. J. Jones, C.-Q. Ma, K. Müllen, P. Bäuerle, A. B. Holmes. *Adv. Funct. Mater.* **20**, 927 (2010).
69. W. W. H. Wong, C.-Q. Ma, W. Pisula, C. Yan, X. L. Feng, D. J. Jones, K. Müllen, R. A. Janssen, P. Bäuerle, A. B. Holmes. *Chem. Mater.* **22**, 457 (2010).
70. W. W. H. Wong, C.-Q. Ma, W. Pisula, A. Mavrinskiy, X. Feng, H. Seyler, D. J. Jones, K. Müllen, P. Bäuerle, A. B. Holmes. *Chem.—Eur. J.* **17**, 5549 (2011).
71. W. W. H. Wong, T. Khoury, D. Vak, C. Yan, D. J. Jones, M. J. Crossley, A. B. Holmes. *J. Mater. Chem.* **20**, 7005 (2010).
72. W. W. H. Wong, D. Vak, T. B. Singh, S. J. Ren, C. Yan, D. J. Jones, I. I. Liaw, R. N. Lamb, A. B. Holmes. *Org. Lett.* **12**, 5000 (2010).
73. E. Clar. *The Aromatic Sextet*, John Wiley, London (1972).
74. G. R. Desiraju, A. Gavezzotti. *Acta Crystallogr., Sect. B* **45**, 473 (1989).
75. G. R. Desiraju, A. Gavezzotti. *Chem. Commun.* 621 (1989).
76. A. Gavezzotti, G. R. Desiraju. *Acta Crystallogr., Sect. B* **44**, 427 (1988).
77. E. Clar, C. T. Ironside, M. Zander. *J. Chem. Soc.* 142 (1959).
78. E. Clar. *Polycyclic Hydrocarbons*, Vol. 2, John Wiley, New York (1964).
79. E. Clar. *Polycyclic Hydrocarbons: Their Synthesis and Reactions*, Vol. 1, John Wiley, New York (1964).
80. J. C. Fetzer. *Large (C>=24) Polycyclic Aromatic Hydrocarbons*, John Wiley, New York (2000).
81. Z. Wang, D. Watson Mark, J. Wu, K. Müllen. *Chem. Commun.* 336 (2004).
82. J. M. Robertson, J. Trotter. *J. Chem. Soc.* 1280 (1961).
83. R. Goddard, M. W. Haenel, W. C. Herndon, C. Krüger, M. Zander. *J. Am. Chem. Soc.* **117**, 30 (1995).
84. Z. Wang, F. Doetz, V. Enkelmann, K. Müllen. *Angew. Chem., Int. Ed.* **44**, 1247 (2005).
85. W. Pisula, Z. Tomovic, C. Simpson, M. Kastler, T. Pakula, K. Müllen. *Chem. Mater.* **17**, 4296 (2005).
86. D. W. Breiby, F. Hansteen, W. Pisula, O. Bunk, U. Kolb, J. W. Andreasen, K. Müllen, M. M. Nielsen. *J. Phys. Chem. B* **109**, 22319 (2005).
87. C.-Y. Liu, A. Fechtenkötter, M. D. Watson, K. Müllen, A. J. Bard. *Chem. Mater.* **15**, 124 (2003).
88. D. Wasserfallen, I. Fischbach, N. Chebotareva, M. Kastler, W. Pisula, F. Jäckel, M. D. Watson, I. Schnell, J. P. Rabe, H. W. Spiess, K. Müllen. *Adv. Funct. Mater.* **15**, 1585 (2005).
89. S. P. Brown, I. Schnell, J. Dietrich Brand, K. Müllen, H. W. Spiess. *J. Mol. Struct.* **521**, 179 (2000).
90. S. P. Brown, I. Schnell, J. Diedrich Brand, K. Müllen, H. W. Spiess. *Phys. Chem. Chem. Phys.* **2**, 1735 (2000).
91. S. P. Brown, I. Schnell, J. Dietrich Brand, K. Müllen, H. W. Spiess. *J. Am. Chem. Soc.* **121**, 6712 (1999).
92. C. Grigoriadis, N. Haase, H.-J. Butt, K. Müllen, G. Floudas. *Adv. Mater.* **22**, 1403 (2010).

© 2012, IUPAC

93. C. Grigoriadis, N. Haase, H.-J. Butt, K. Müllen, G. Floudas. *Soft Matter* **7**, 4680 (2011).
94. W. Pisula, Z. Tomovic, B. El Hamaoui, M. D. Watson, T. Pakula, K. Müllen. *Adv. Funct. Mater.* **15**, 893 (2005).
95. M. Kastler, W. Pisula, D. Wasserfallen, T. Pakula, K. Müllen. *J. Am. Chem. Soc.* **127**, 4286 (2005).
96. T. Yamamoto, T. Fukushima, A. Kosaka, W. Jin, Y. Yamamoto, N. Ishii, T. Aida. *Angew. Chem., Int. Ed.* **47**, 1672 (2008).
97. W. Jin, Y. Yamamoto, T. Fukushima, N. Ishii, J. Kim, K. Kato, M. Takata, T. Aida. *J. Am. Chem. Soc.* **130**, 9434 (2008).
98. Y. Yamamoto, T. Fukushima, Y. Suna, N. Ishii, A. Saeki, S. Seki, S. Tagawa, M. Taniguchi, T. Kawai, T. Aida. *Science* **314**, 1761 (2006).
99. Y. Yamamoto, T. Fukushima, W. Jin, A. Kosaka, T. Hara, T. Nakamura, A. Saeki, S. Seki, S. Tagawa, T. Aida. *Adv. Mater.* **18**, 1297 (2006).
100. W. Jin, T. Fukushima, M. Niki, A. Kosaka, N. Ishii, T. Aida. *Proc. Natl. Acad. Sci. USA* **102**, 10801 (2005).
101. W. Jin, T. Fukushima, A. Kosaka, M. Niki, N. Ishii, T. Aida. *J. Am. Chem. Soc.* **127**, 8284 (2005).
102. N. Reitzel, T. Hassenkam, K. Balashev, T. R. Jensen, P. B. Howes, K. Kjaer, A. Fechtenkötter, N. Tchebotareva, S. Ito, K. Müllen, T. Bjornholm. *Chem.—Eur. J.* **7**, 4894 (2001).
103. H. C. Hesse, D. Lembke, L. Dossel, X. Feng, K. Müllen, L. Schmidt-Mende. *Nanotechnology* **22**, 055303 (2011).
104. M. Keil, P. Samori, D. A. dos Santos, J. Birgerson, R. Friedlein, A. Dkhissi, M. Watson, K. Müllen, J. L. Bredas, J. P. Rabe, W. R. Salaneck. *J. Chem. Phys.* **116**, 10854 (2002).
105. K. Mukai, M. Harada, Y. Kikuzawa, T. Mori, J. Sugiyama. *Electrochem. Solid-State Lett.* **14**, A52 (2011).
106. A. C. Grimsdale, J. Wu, K. Müllen. *Chem. Commun.* 2197 (2005).
107. A. Okabe, M. Niki, T. Fukushima, T. Aida. *Chem. Lett.* **35**, 228 (2006).
108. S. Yang, X. Feng, L. Zhi, Q. Cao, J. Maier, K. Müllen. *Adv. Mater.* **22**, 838 (2010).
109. Y. Zilberman, U. Tisch, G. Shuster, W. Pisula, X. Feng, K. Müllen, H. Haick. *Adv. Mater.* **22**, 4317 (2010).
110. Y. Zilberman, U. Tisch, W. Pisula, X. Feng, K. Müllen, H. Haick. *Langmuir* **25**, 5411 (2009).
111. W. Pisula, X. Feng, K. Müllen. *Chem. Mater.* **23**, 554 (2010).
112. A. M. van de Craats, J. M. Warman. *Adv. Mater.* **13**, 130 (2001).
113. J. M. Warman, A. M. Van De Craats. *Mol. Cryst. Liq. Cryst.* **396**, 41 (2003).
114. A. M. Van De Craats, J. M. Warman, A. Fechtenkötter, J. Dietrich Brand, M. A. Harbison, K. Müllen. *Adv. Mater.* **11**, 1469 (1999).
115. A. M. Van de Craats, J. M. Warman, K. Müllen, Y. Geerts, J. Dietrich Brand. *Adv. Mater.* **10**, 36 (1998).
116. J. Piris, M. G. Debije, N. Stutzmann, B. W. Laursen, W. Pisula, M. D. Watson, T. Bjornholm, K. Müllen, J. M. Warman. *Adv. Funct. Mater.* **14**, 1053 (2004).
117. J. Piris, M. G. Debije, N. Stutzmann, A. M. van de Craats, M. D. Watson, K. Müllen, J. M. Warman. *Adv. Mater.* **15**, 1736 (2003).
118. I. O. Shklyarevskiy, P. Jonkheijm, N. Stutzmann, D. Wasserberg, H. J. Wondergem, P. C. M. Christianen, A. P. H. J. Schenning, D. M. de Leeuw, Z. Tomovic, J. Wu, K. Müllen, J. C. Maan. *J. Am. Chem. Soc.* **127**, 16233 (2005).
119. H. N. Tsao, H. J. Räder, W. Pisula, A. Rouhanipour, K. Müllen. *Phys. Status Solidi A* **205**, 421 (2008).
120. W. Pisula, Z. Tomovic, M. Stepputat, U. Kolb, T. Pakula, K. Müllen. *Chem. Mater.* **17**, 2641 (2005).
121. W. Pisula, A. Menon, M. Stepputat, I. Lieberwirth, U. Kolb, A. Tracz, H. Sirringhaus, T. Pakula, K. Müllen. *Adv. Mater.* **17**, 684 (2005).

122. T. Mori, H. Takeuchi, H. Fujikawa. *J. Appl. Phys.* **97**, 066102 (2005).
123. J. M. Warman, J. Piris, W. Pisula, M. Kastler, D. Wasserfallen, K. Müllen. *J. Am. Chem. Soc.* **127**, 14257 (2005).
124. Q. Zhang, P. Prins, S. C. Jones, S. Barlow, T. Kondo, Z. An, L. D. A. Siebbeles, S. R. Marder. *Org. Lett.* **7**, 5019 (2005).
125. P. Samori, A. Fechtenkötter, E. Reuther, M. D. Watson, N. Severin, K. Müllen, J. P. Rabe. *Adv. Mater.* **18**, 1317 (2006).
126. X. J. Zhang, X. X. Jiang, K. Zhang, L. Mao, J. Luo, C. Y. Chi, H. S. O. Chan, J. S. Wu. *J. Org. Chem.* **75**, 8069 (2010).
127. M. Kastler, F. Laquai, K. Müllen, G. Wegner. *Appl. Phys. Lett.* **89**, 252103 (2006).
128. A. Rybak, J. Pfleger, J. Jung, M. Pavlik, I. Glowacki, J. Ulanski, Z. Tomovic, K. Müllen, Y. Geerts. *Synth. Met.* **156**, 302 (2006).
129. A. J. Mozer, C. Q. Ma, W. W. H. Wong, D. J. Jones, P. Bäuerle, G. G. Wallace. *Org. Electron.* **11**, 573 (2010).
130. L. Schmidt-Mende, M. D. Watson, K. Müllen, R. H. Friend. *Mol. Cryst. Liq. Cryst.* **396**, 73 (2003).
131. L. Schmidt-Mende, A. Fechtenkötter, K. Müllen, E. Moons, R. H. Friend, J. D. MacKenzie. *Science* **293**, 1119 (2001).
132. J. P. Schmidtke, R. H. Friend, M. Kastler, K. Müllen. *J. Chem. Phys.* **124**, 174704 (2006).

© 2012, IUPAC